Molecular Catalysis 509 (2021) 111603

Contents lists available at ScienceDirect

Molecular Catalysis

journal homepage: www.journals.elsevier.com/molecular-catalysis

Hydrothermal self - sacrificing growth of polymorphous MnO_2 on magnetic porous - carbon (Fe_3O_4@Cg/MnO_2): A sustainable nanostructured catalyst for activation of molecular oxygen

Zohreh Bakhtiarzadeh [b], Shamila Rouhani [c], Ziba Karimi [b], Sadegh Rostamnia [a,b,*], Titus A. M. Msagati [c], Dokyoon Kim [d], Ho Won Jang [e], Seeram Ramakrishna [f], Rajender S. Varma [g,*], Mohammadreza Shokouhimehr [e,*]

[a] Organic and Nano Group (ONG), Department of Chemistry, Iran University of Science and Technology (IUST), PO Box 16846-13114, Tehran, Iran
[b] Organic and Nano Group (ONG), Department of Chemistry, Faculty of Science, University of Maragheh, PO BOX 55181-83111, Maragheh, Iran
[c] Institute for Nanotechnology and Water Sustainability (iNanoWS), College of Science, Engineering and Technology, University of South Africa, Johannesburg 1709, South Africa
[d] Department of Bionano Engineering, Hanyang University, Ansan 15588, Republic of Korea
[e] Department of Materials Science and Engineering, Research Institute of Advanced Materials, Seoul National University, Seoul, 08826, Republic of Korea
[f] Department of Mechanical Engineering, Center for Nanofibers and Nanotechnology, National University of Singapore, Singapore, 119260, Singapore
[g] Regional Center of Advanced Technologies and Materials, Czech Advanced Technology and Research Institute, Palacky University, Šlechtitelů 27, 783 71 Olomouc, Czech Republic

ARTICLE INFO

Keywords:
MnO_2
Magnetic nanoparticles
Alcohol oxidation
Nanostructured catalyst

ABSTRACT

Novel core-shell carbon coated-magnetic (Fe_3O_4@C_g) nanoparticles supported MnO2 nanosheets (with α- and β-type structure) (Fe_3O_4@C_g/MnO_2) are synthesized through a self-sacrificing templet method. The new hybrid material was fully characterized with Fourier transformed infrared spectroscopy, energy-dispersive X-ray spectroscopy, scanning electron microscopy, X-ray diffraction analysis (XRD), N_2 adsorption/desorption analysis, and transmission electron microscopy; XRD and SEM results affirmed that α- and β-MnO_2 nanosheets polymorphs onto the Fe_3O_4@C_g. The catalytic activity of the as-prepared nanostructured catalyst Fe_3O_4@C_g/MnO_2 has been evaluated in O_2 activation for the selective oxidation of benzyl alcohol to benzaldehyde with high conversion; it stability being confirmed by the recycling of the nanostructured catalyst with no obvious loss even after six repeated runs.

1. Introduction

Nowadays, intensive efforts have been made to meet the ever-growing demands for the development of greener catalytic protocols with high-efficiency and high-selectivity [1,2]. Presently, the preparation of aldehydes by selective alcohol oxidation is a pivotal chemical transformation for the synthesis of a variety of vital intermediates for the fine chemicals [3]. Traditionally, the alcohol oxidation procedures are performed with stoichiometric amounts of high-cost inorganic oxidants which leads to the formation of environmentally harmful by-products [4]. Hence, the development of green, efficient and economic heterogeneous catalytic aerobic oxidation systems exploiting the low-cost O_2 or air as a terminal oxidant would be ideally suited for such significant chemical transformations [5–7].

In recent years, heterogeneous catalytic system for the oxidation of benzyl alcohol (BzOH) over both, the noble and non-noble transition metal oxides have been studied extensively; deployment of non-noble metal oxides has remarkable advantageous over noble metals due to their inexpensive nature and high availability [8]. Among the various non-noble transition metal oxides, manganese oxides have attracted increasing attention due to the earth-abundant sources, high catalytic activity, rich structures and morphologies, low-cost and environmental friendliness, therefore, they have been widely applied in the fields of lithium batteries, oxidants, and in catalysis arena [9–12].

Manganese oxide exits in various crystal structure forms such as α, β and λ - types which differ in the arrangement of the basic octahedral [MnO_6] unit [13]. Recently, much attention has been directed toward the synthesis of polymorphs of MnO_2 with different morphology owing

* Corresponding author.
E-mail addresses: rostamnia@iust.ac.ir (S. Rostamnia), varma.rajender@epa.gov (R.S. Varma), mrsh2@snu.ac.kr (M. Shokouhimehr).

https://doi.org/10.1016/j.mcat.2021.111603
Received 22 December 2020; Received in revised form 8 April 2021; Accepted 23 April 2021
Available online 28 May 2021

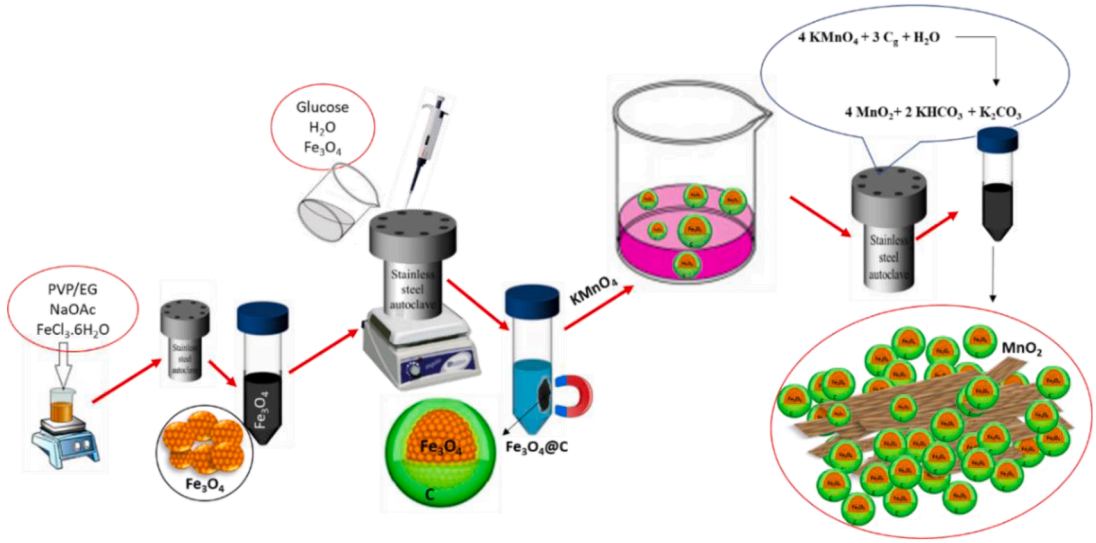

Fig. 1. Schematic preparation of MnO_2 on CHC substrate by hydrothermal method.

to the varied applications of polymorphism in the chemical industry [9, 14–17]. Among MnO_2 phases, α- and β-MnO_2 are less active catalytically in comparison to γ-phase which lead to the formation of desirable oxidation products [18]; MnO_2 has been reported as a selective oxidizing catalyst in the aerobic oxidation of BzOH with high reactivity and selectivity [19–24].

Overall, the nanoparticles (NPs) exhibit excellent catalytic performances due to the size effect and their large surface area. However, the use of NPs as a catalyst is associated with some limitations as it suffers from aggregations and low stability [18,25]. The aforementioned challenges for NPs need viable solutions and not surprisingly, researchers have suggested that immobilizing active species onto an ideal support could solve the lingering problem [22,26–28]. Recently, Hu et al. reported the synthesis of ultrafine MnO_2 NPs supported on graphene oxide, which was applied as a catalyst in selective aerobic oxidation of BzOH [8]. Wu and co-workers utilized the supported manganese oxide on MCM-41 zeolite as a catalyst to oxidize BzOH [29]. Another study was reported by Kadam et al., where λ -MnO_2/GO composite was employed for the oxidation of BzOH [18].

Core-shell magnetic NPs have garnered considerable attention lately due to their multi-functional properties such as large accessible surface area, biocompatibility, low toxicity, easy surface decoration, high stability and easy separation which render them as ideal materials for catalytic applications [30,31].

Therefore, in continuation of our research interest in exploring efficient catalysts [32–35], the preparation of core-shell carbon-coated magnetic NPs via a facile hydrothermal method is described that could be utilized as a support for the immobilization of α- β- and δ-MnO_2 (Fe_3O_4@C_g/MnO_2). Subsequently, it was employed as a recyclable catalyst for selective aerobic oxidation of BzOH into the corresponding aldehyde. Furthermore, a controlled oxidation of alcohols was accomplished with no over-oxidation to carboxylic acid (ArCOOH) which can be related to the presence of α- and β-MnO_2 polymorphs. The synthesis of MnO_2 nanosheets have been generally performed using $KMnO_4$ and $MnCl_2$/MnS as a metal source [13,9]. It is worth mentioning that the Fe_3O_4@C_g/MnO_2 was prepared by in-situ growing method via self-sacrificing carbon shell layer as reducing agent with $KMnO_4$ providing a Mn-source [9,36]. Moreover, Fe_3O_4 NPs were simply prepared using iron (III) chloride as the only ferric ion single resource (Scheme 1).

The aerobic oxidation of BzOH and its derivatives by Fe_3O_4@C_g/MnO_2 show that the corresponding aldehydes can be obtained in high yield as the main products. The Fe_3O_4@C_g/MnO_2 catalyst could also be reused for six runs without any significant loss of catalytic activity. The advantage of this aerobic oxidation method includes the simple operation, easy catalyst separation and reusability, and high selectivity.

2. Experimental

2.1. Materials

All chemicals including iron (III) chloride hexahydrate ($FeCl_3$•$6H_2O$), potassium permanganate ($KMnO_4$), poly(vinylpyrrolidone) (PVP), ethylene glycol, benzyl alcohol, sodium acetate and glucose were obtained from Merck and used without further purification. All other chemicals were of analytical grade purity and used without further purification.

2.2. Synthesis of carbon-coated Fe_3O_4 NPs (Fe_3O_4@C_g)

The Fe_3O_4 NPs were first synthesized via a modified hydrothermal method. $FeCl_3$. $6H_2O$ (1.5 g), polyvinyl pyrrolidine (PVP) (1 g) and sodium acetate (2 g) were dissolved in ethylene glycol (30 mL) and stirred for 1 h. Then the mixture was transferred into a Teflon-lined stainless-steel autoclave and heated at 200 °C for 10 h. After cooling to room temperature, the Fe_3O_4 NPs were separated by using an external magnet, washed with distilled water and ethanol several times and dried under reduced pressure. In the next stage, the synthesis of magnetite-carbon core-shell NPs was accomplished through sonicating the as-fabricated Fe_3O_4 NPs with 5 g glucose in 30 mL deionized water. Next, the above mixture was transferred into a Teflon-lined stainless-steel autoclave, sealed and kept at a temperature of 200 °C for 12 h. After the reaction system was cooled to ambient temperature, the ensuing black precipitate was separated by a magnetic field, washed with distilled water and methanol, and finally dried in a vacuum oven.

2.3. Synthesis of Fe_3O_4@C_g/MnO_2

MnO_2 nanosheets supported onto the Fe_3O_4@C_g NPs were assembled by dispersing the Fe_3O_4@C_g (0.3 g) in 75 mL aqueous solution of $KMnO_4$ (0.03 M) with ultrasonication for 1 h. Then, the resulting mixture was transferred into a Teflon-lined stainless-steel autoclave and heated at 180 °C for 6 h. The obtained product was separated, and washed thoroughly with water and methanol before being dried in an oven, providing the Fe_3O_4@C_g/MnO_2 nanostructured catalyst.

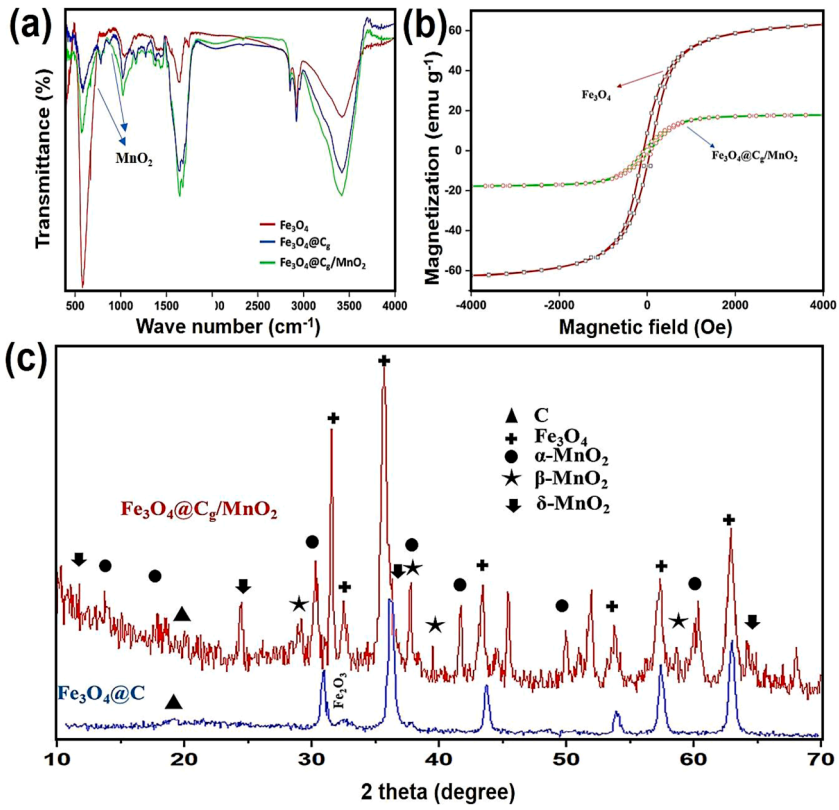

Fig. 2. (a) FTIR spectra of Fe_3O_4, $Fe_3O_4@C_g$, and $Fe_3O_4@C_g/MnO_2$. (b) VSM magnetization curves of Fe_3O_4 and $Fe_3O_4@C_g/MnO_2$. (c) XRD patterns of $Fe_3O_4@C_g$ and $Fe_3O_4@C_g/MnO_2$.

2.4. A typical procedure for O_2-activation for selective oxidation of BzOH in the presence of $Fe_3O_4@C_g/MnO_2$

BzOH (1 mmol) and $Fe_3O_4@C_g/MnO_2$ (0.05 g) were dissolved in 10 mL of toluene under continuous purging of dry air. Then, the reaction was stirred at 120 °C for 4 h. After completion of the reaction, the catalyst was separated from the solution using an external magnet, washed, and dried under reduced pressure. The conversion of the products was calculated as follows:

$$\text{Conversion } (\%) = \left(\frac{C_o - C_y}{C_o}\right) \times 100$$

where, C_o is the initial concentration of alcohols. C_y is the concentrations of alcohols at a certain reaction time. The yields of products were calculated via the normalization method based on the GC–MS analysis. Turnover number (TON) represents the average number of substrate molecules converted into the product per molecule of the catalyst (Table 2).

3. Result and discussion

The preparation of $Fe_3O_4@C_g/MnO_2$ is implemented via an effective strategy as depicted in Fig. 1. The superparamagnetic $Fe_3O_4@C_g$ was first fabricated via a solvothermal route by applying ferric ion as a single iron source. Then, polymorphous MnO_2 nanosheets were grown in the presence of $Fe_3O_4@C_g$ through self-sacrificing redox reaction between carbon shell layer and $KMnO_4$ [37]. The oxidation/reduction reaction is described in the equation shown in Fig. 1.

Fig. 2a shows the Fourier transform infrared (FTIR) spectrums of Fe_3O_4, $Fe_3O_4@C_g$, and $Fe_3O_4@C_g/MnO_2$. The sharp intense band at 570 cm^{-1} is assigned to the vibration of the Fe–O group which confirms the presence of the Fe_3O_4. The broad peaks at 3420 cm^{-1} can be assigned to O–H stretching vibration arising from hydroxyl groups [38]. The band observed at 1024 cm^{-1} can be attributed to the C—O stretching vibration. Peaks at 1646 and 1679 cm^{-1} frequencies represent the stretching vibration of $C = C$ and COOH groups, respectively [39]. In addition, the peak signals at 2850 and 2921 cm^{-1} correspond to the asymmetric and symmetric C—H vibration. These numerous absorption bands indicate the amount of various carbon and oxygen-containing functional groups on the surface of the $Fe_3O_4@C_g$ have been obtained from the glucose during the hydrothermal synthesis [40]. Moreover, for the $Fe_3O_4@C_g/MnO_2$, the peaks at 765, 621 and 530 cm^{-1} are associated to the Mn-O stretching vibration which affirms the presence of polymorphous MnO_2.

The superparamagnetic behavior of magnetic NPs is favourable for the magnetic separation. Hence, the magnetic properties of Fe_3O_4 and $Fe_3O_4@C_g/MnO_2$ were investigated using a vibrating sample magnetometer (VSM) at room temperature; the hysteresis curves in Fig. 2b shows the saturation magnetization of Fe_3O_4 NPs to be ~64 emu/g, while $Fe_3O_4@C_g/MnO_2$ has a magnetization of ~18 emu/g. The decreased saturation magnetization value of $Fe_3O_4@C_g/MnO_2$ is attributed to the surface modification of the NPs. Nonetheless, it is still good enough for facilitating the magnetic separation of particles.

To confirm the polymorphous phases of the as-obtained $Fe_3O_4@C_g/MnO_2$, X-ray diffraction analysis (XRD) analysis was performed (Fig. 2c) which shows a series of characteristic peaks at 30.3, 35.4, 43.6, 53.4, 57.3, and 63.2° (2θ) which are in good consistent with the cubic spinel phase of Fe_3O_4 (JCPDS card No. 19–0629). Moreover, arising broad peak (19.5°) beside the iron oxide peak can be ascribed to the specific reflection of amorphous carbons [41]. In $Fe_3O_4@C_g/MnO_2$, by comparing to the XRD patterns of the standard α- and β-MnO_2 (JCPDS card No. 44–0141 and No. 24–0735) samples, it can be realized that the hydrothermally *in-situ* growing manganese oxide were polymorphs of MnO_2 with α, β and δ phase structures. In addition, on the basis of these results, it is revealed that the core-shell carbon-coated Fe_3O_4 NPs has not changed during growth process of MnO_2 nanosheets.

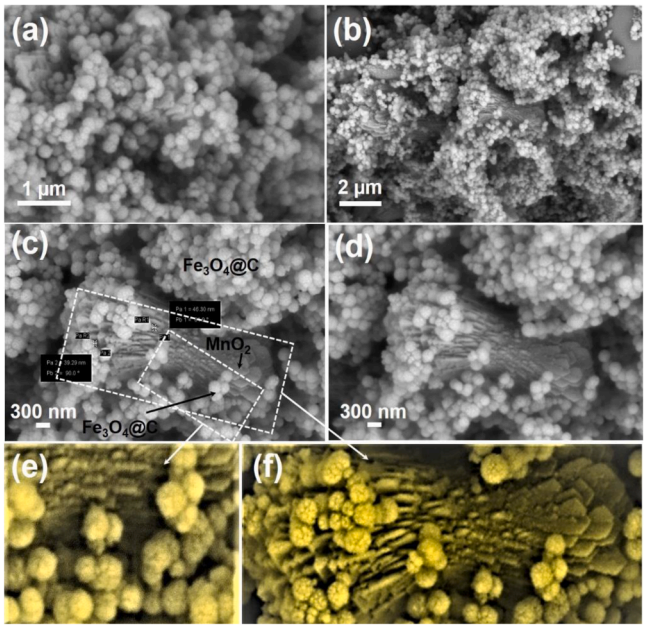

Fig. 3. SEM images of (a,b) $Fe_3O_4@C_g$, (c,d) $Fe_3O_4@C_g/MnO_2$, and (e,f) $Fe_3O_4@C_g$ and MnO_2.

The morphology and nanostructure of $Fe_3O_4@C_g$ NPs and $Fe_3O_4@C_g/MnO_2$ were studied by scanning electron microscopy (SEM) and transmission electron microscopy (TEM) analysis. The SEM images displays that the $Fe_3O_4@C_g$ NPs, prepared via solvothermal method, have spherical structure and uniform sizes with the diameter of 200–220 nm (Fig. 3a,b). Fig. 3c-f reveal that the polymorphous MnO_2 may be formed by several MnO_2 nanosheets overlapping together on the surfaces of $Fe_3O_4@C_g$.

As is clear from the TEM image with higher magnification (Fig. 4a-e), the $Fe_3O_4@C_g$ NPs have a core-shell structure comprising aggregated Fe_3O_4 (dark core) encapsulated with amorphous carbon shell of 21.69 nm of thickness (light area) which is less dense than the core structure. The results from the TEM image of $Fe_3O_4@C_g/MnO_2$ (Fig. 4d,e) confirmed that MnO_2 nanosheets are located on the surface of spherical $Fe_3O_4@C_g$ NPs.

The energy-dispersive X-ray spectroscopy (EDX) shows the presence of the expected elements in the structure of the catalyst, comprising oxygen, carbon, iron and manganese in the $Fe_3O_4@C_g/MnO_2$ (Fig. 5a). The investigation of the specific surface area for $Fe_3O_4@C_g$ was performed using BET measurement as presented in Fig. 5b. It can be seen that carbon-coated Fe_3O_4 NPs have the BET surface area of 12 m^2/g.

The catalytic performance of $Fe_3O_4@C_g/MnO_2$ was evaluated in the selective oxidation of BzOH to benzaldehyde (BzCHO) with O_2 as an oxidant for 4 h in various solvents, under different reaction temperature and the amounts of the nanostructured catalyst; obtained results are summarized in Table 1. As seen in Table 1, the conversion of BzOH to

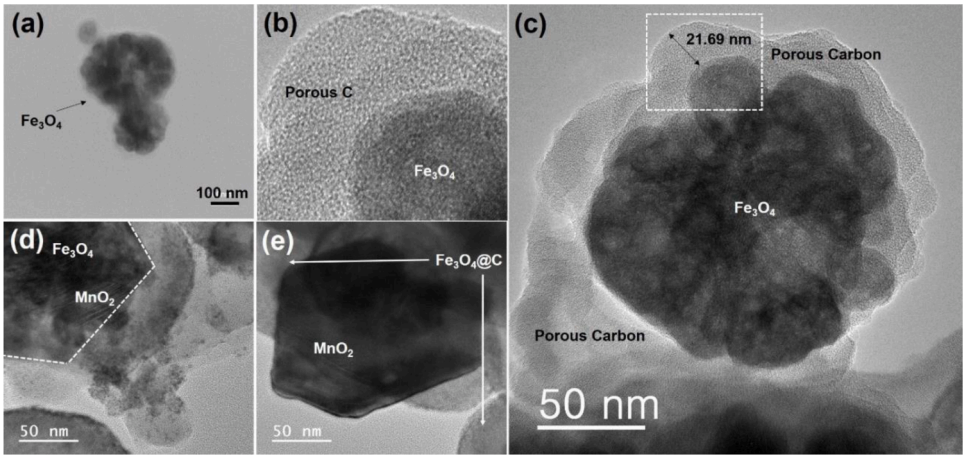

Fig. 4. High magnification TEM images of (a) Fe_3O_4, (b,c) $Fe_3O_4@C_g$, and (d,e) $Fe_3O_4@C_g/MnO_2$.

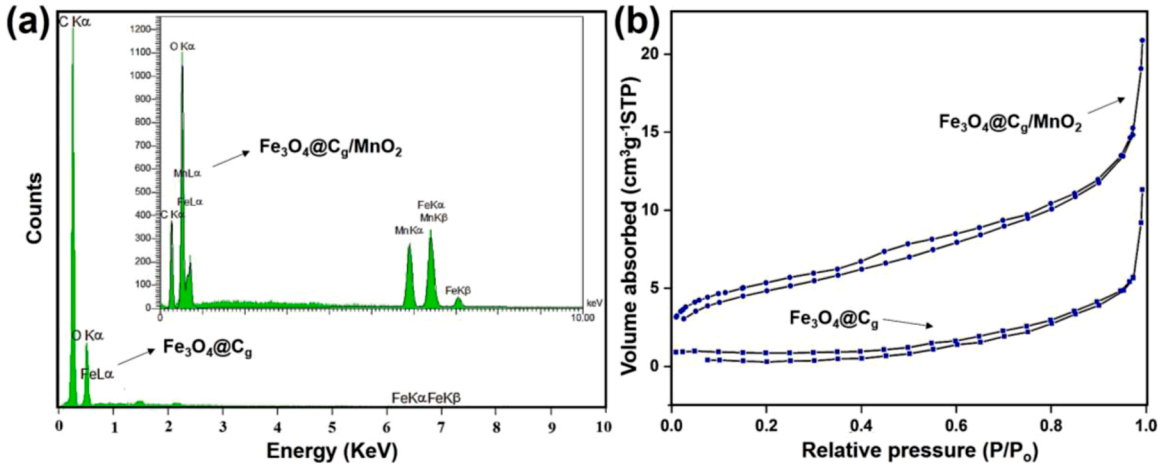

Fig. 5. (a) EDX spectra of $Fe_3O_4@C_g/MnO_2$ and $Fe_3O_4@C_g$. (b) N_2 Adsorption–desorption isotherms of $Fe_3O_4@C_g/MnO_2$ and $Fe_3O_4@C_g$.

Table 1
BzOH oxidation by $Fe_3O_4@C_g/MnO_2$ under various reaction conditions[a].

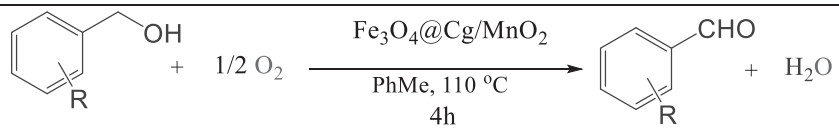

Entry	Substrate	Conv. [b] (%)	Yield [b] (%)	TON [c]	TOF [d] (h^{-1})
1	4-Br	88	86	-	-
2	4-Cl	91	88	48	12
3	4-Me	90	90	-	-
4	3-NO_2	78	74	-	-
5	2-Cl	81	76	-	-
6	4-MeO	94	92	-	-
7	3,4,5-MeO	95	92	-	-
8	H	96	92	53	13.25
9	2-Me	76	73	-	-
10	2-Cl	65	58	-	-
11	3-Cl	89	86	-	-

Entry	Catalyst (mg)	Solvent	Temperature (°C)	Conversion/Yield[b] (%)
1	5	Toluene	110	40/38
2	10	Toluene	110	82/76
3	20	Toluene	110	96/92
4	30	Toluene	70	64/60
5	20	CH_2Cl_2	100	50/48
6	20	$CHCl_3$	100	30/28
7	20	H_2O	100	70/45
8	20	Toluene	r.t	10/-
9	20	Toluene	30	25/-
10	20	Toluene	50	60/54
11	20	Toluene[d]	110	-/trace

[a]Reaction conditions: BzOH (1 mmol), $Fe_3O_4@C_g/MnO_2$, solvent (10 mL), 110 °C, 4 h.
[b]Based on GC–MS.
[c]Sealed tube.
[d]Without BzOH for oxidation evaluation of toluene to BzCHO.

Table 2
Results of selective benzylic alcohols oxidation over $Fe_3O_4@C_g/MnO_2$[a].

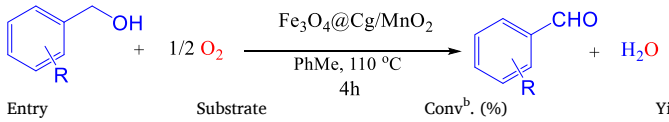

Entry	Substrate	Conv[b]. (%)	Yield[b] (%)	TON[c]	TOF[d] (h^{-1})
1	4-Br	88	86	–	–
2	4-Cl	91	88	48	12
3	4-Me	90	90	–	–
4	3-NO_2	78	74	–	–
5	2-Cl	81	76	–	–
6	4-MeO	94	92	–	–
7	3,4,5-MeO	95	92	–	–
8	H	96	92	53	13.25
9	2-Me	76	73	–	–
10	2-Cl	65	58	–	–
11	3-Cl	89	86	–	–

[a]Reaction conditions: BzOH (1 mmol), $Fe_3O_4@C_g/MnO_2$ (20 mg), Toluene (10 mL), 110 °C, 4 h with O_2 balloon.
[b]Based on GC–MS.
[c]Turnover number represents the average number of substrate molecules converted into the product per molecule of catalyst.
[d]Turnover frequency per hour.

BzCHO was gradually enhanced with the increase of the amount of catalyst (Table 1, entries 1–3). Indeed, 20 mg of $Fe_3O_4@C_g/MnO_2$ showed the highest conversion (94%). In order to study the effect of the solvents, the reaction was conducted in various solvents such as CH_2Cl_2, $CHCl_3$, toluene and H_2O under the same reaction conditions. Among the applied solvents, the highest conversion was observed in toluene (Table 1, entry 8). The influence of reaction temperature was studied for the optimized catalyst system. As indicated in Table 1, at a lower temperature (<50 °C) conversion were rather low (< 60%), whereas at the elevated temperature of 120 °C, the BzOH conversion was markedly increased (up to 96%); hence it was found that the high temperature was favourable for the oxidation of BzOH. Furthermore, the corresponding

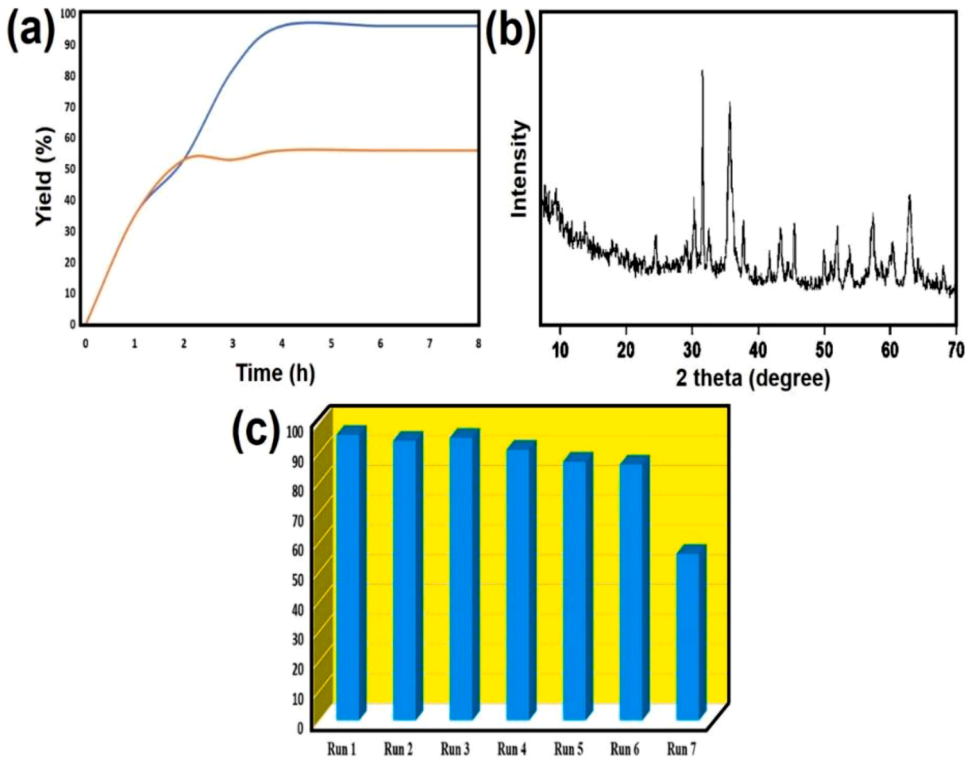

Fig. 6. (a) Leaching test of Fe_3O_4@Cg/MnO_2. (b) XRD pattern of the recovered Fe_3O_4@C_g/MnO_2 catalyst. (c) Recycling of Fe_3O_4@C_g/MnO_2 catalyst for the oxidation of BzOH to BzCHO in toluene under oxygen atmosphere at 110 °C for 4 h.

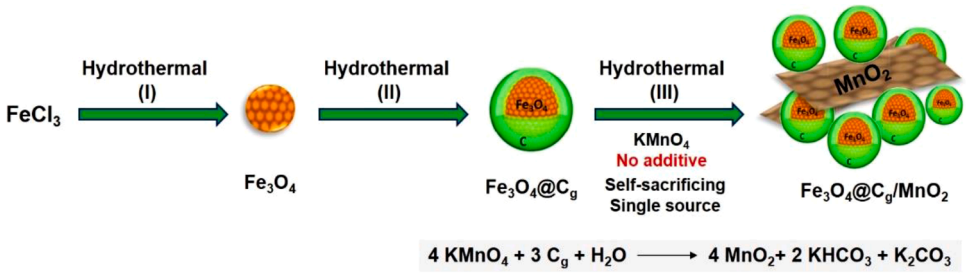

Scheme 1. Procedure for the synthesis of Fe_3O_4@C_g/MnO_2.

aldehyde could be obtained as the only desirable product with yield of 21%, 15% and 12% by using MnO_2, Fe_3O_4, and Fe_3O_4@C_g as a catalyst under the same reaction conditions, respectively. When we did not charge the reaction mixture with BzOH to check oxidation of toluene, no formation of formation of BzOH or BzCHO could be detected (Table 1, entry 11).

To demonstrate the applicability of the as-fabricated nanostructured catalyst, the optimized reaction conditions (20 mg of Fe_3O_4@C_g/MnO_2, Toluene, 110 °C) were chosen for a further study of the catalyst in the oxidation of various benzylic alcohols with different electron-withdrawing and electron-donating substituents (Table 2). The results revealed that electronic properties of substitutes on benzyl group have an impact on the oxidation reaction. In presence of electron-donating groups (Table 2, entries 3,6,7), the corresponding BzCHO products were obtained in higher conversions than the electron-withdrawing groups (Table 2, entries 1,2,4) over 4 h. The effect of the position (meta, ortho and para) of electron-withdrawing substituents on this reaction was also assessed; higher conversion was obtained for meta-position because of the apparent steric hindrance and electronic nature of ortho and para position, respectively (Table 2, entries 3–5). It should be noted that this method is highly selective for the oxidation of benzyl alcohols to the corresponding aldehydes, without any detectable over-oxidation to their carboxylic acids.

In the hot filtration leaching test, the Fe_3O_4@C_g/MnO_2 nanostructured catalyst was removed in the middle of the reaction (2 h) and the reaction was continued with the reaction mixture without the nanostructured catalyst. It was observed that there is no enhancement in the conversion to aldehyde yield, thus indicating that no active species were leached during the reaction mixture (Fig. 6a). The recovery and reusability experiments for the selective oxidation of BzOH was also performed by six successive cycles under the optimum conditions to evaluate the stability of the Fe_3O_4@C_g/MnO_2 nanostructured catalyst (Fig. 6c). After the completion of the reaction, the nanostructured catalyst was separated using an external magnet, washed thoroughly with methanol, and then dried for the next run. Then, the remaining magnetic nanostructured catalyst was also deployed under the same experimental reaction conditions. It is worth pointing out that the Fe_3O_4@C_g/MnO_2 could be reused at least six times without appreciable reduction in conversions of BzOH to BzCHO. As depicted in Fig. 6b, the XRD pattern of the recovered Fe_3O_4@C_g/MnO_2 catalyst ascertained that no change in the phase composition occurred compared to fresh nanostructured catalyst. These findings confirm that the structure of the

Table 3
Catalytic activity of various Mn-based catalysts for the oxidation of BzOH.

Entry	Catalyst	Conditions	Temperature (°C)	Time (h)	Yield (%) [Refs.]
1	Ni_2Mn-LDH (0.2 mg)	BzOH1 mmol, O_2 (1 atm)	120	1.7	99 [24]
2	Ce/MnO_x (450 mg)	BzOH 10 mM, O_2 flow (60 mL/min)	70	2	81 [42]
3	MnO_2 NPs@GO (200 mg)	BzOH 100 mM, air flow (200 mL/min)	110	2	83 [8]
4	Au/MnO_2 (20 mg)	BzOH 2 g, O_2 1 bar	120	2	6 [43]
5	Co_3O_4/MnO2 (25 mg)	BzOH 100 Mm, O_2 flow (20 mL/min)	100	12	92 [44]
6	Pd@Mn_5O_8 (80 mg)	BzOH 100 mM, TBHP	80	4	89 [19]
7	MnO_2—Co (67 mg/mmol)	BzOH Toluene O_2 aerobic	110	4	89 [20]
8	Fe_3O_4@C_g/MnO_2 (20 mg)	BzOH 1 mmol, Toluene, O_2 aerobic	110	4	92 [This work]

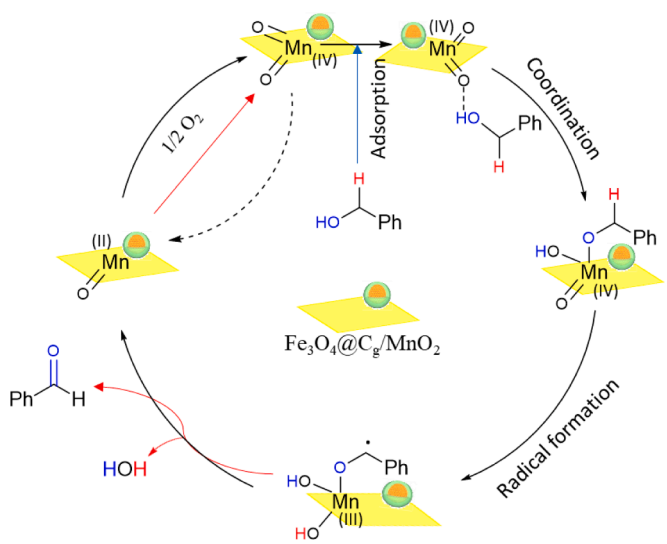

Scheme 2. Proposed mechanism for the oxidation of BzOH by Fe_3O_4@C_g/MnO_2 catalyst.

Fe_3O_4@C_g/MnO_2 has excellent stability under the reaction conditions which are of great significance for practical applications.

Table 3 summarizes the catalytic activity studies of several previously published Mn-base catalysts. The Fe_3O_4@C_g/MnO_2 catalyst exhibited high catalytic activity with good yield in comparison with those selective stipulated studies.

A plausible mechanism for the selective oxidation of BzOH to the corresponding BzCHO by Fe_3O_4@C_g/MnO_2 is outlined in Scheme 2. The process involves free radical mechanism as reported by Goldman [45]. In the first step, the O—H group of the BzOH is added to MnO_2 species to generate a coordination complex. Subsequently, the hydrogen atom transfers from benzylic carbon to oxygen of MnO_2 to produce a stable radical. Finally, by the reduction of the Mn (III) to the more stable Mn (II), the aldehyde product is formed.

4. Conclusions

In the present study, a novel methodology was designed *via* self-sacrificing template route for the growth of polymorphous α- and β-MnO_2 nanosheets onto the core-shell carbon-coated Fe_3O_4 NPs. The ensuing catalyst was characterized by various technique including FTIR, EDX, SEM, TEM, XRD, and BET. Then, the Fe_3O_4@C_g/MnO_2 was applied as a highly active and efficient catalyst for the selective oxidation of BzOH to BzCHO using oxygen as a green oxidant. The results showed that the products were obtained in high conversion over 4 h. The newly developed nanostructured catalyst could also be recycled and reused for six runs without any significant loss of catalytic activity and stability. The significant advantages of this method include the simplicity in operation, simply work-up, excellent selectivity and the reusability.

Declaration of Competing Interest

We wish to confirm that there are no known conflicts of interest associated with this publication and there has been no significant financial support for this work that could have influenced its outcome.

Acknowledgements

This research was supported by the National Research Foundation of Korea (NRF) funded by the Ministry of Science and ICT (2020M2D8A206983011). Furthermore, the financial supports of the Basic Science Research Program (2017R1A2B3009135) through the National Research Foundation of Korea is appreciated .

Supplementary materials

Supplementary material associated with this article can be found, in the online version, at doi:10.1016/j.mcat.2021.111603.

References

[1] A.G. Moaser, A. Ahadi, S. Rouhani, B.B. Mamba, T.A.M. Msagati, S. Rostamnia, T. Kavetskyy, S. Dugheri, S. Khaksar, A. Hasanzadeh, M. Shokouhimehr, Curbed of molybdenum oxido-diperoxido complex on ionic liquid body of mesoporous Bipy-PMO-IL as a promising catalyst for selective sulfide oxidation, J. Mol. Liq. 312 (2020), 113388, https://doi.org/10.1016/j.molliq.2020.113388.
[2] S. Rostamnia, B. Gholipour, X. Liu, Y. Wang, H. Arandiyan, NH_2 -coordinately immobilized tris (8-quinolinolato) iron onto the silica coated magnetite nanoparticle : Fe_3O_4 @ SiO_2 -FeQ_3 as a selective fenton- like catalyst for clean oxidation of sulfides, J. Colloid Interface Sci. 511 (2018) 447–455, https://doi.org/10.1016/j.jcis.2017.10.028.
[3] M. Guan, C. Wang, J. Zhang, Y. Zhao, Practical organic solvent-free $Cu(OAc)_2$/DMAP/TEMPO-catalyzed aldehyde and imine formation from alcohols under air atmosphere, RSC Adv 4 (2014) 48777–48782, https://doi.org/10.1039/c4ra09851j.
[4] A. Dijksman, I.W.C.E. Arends, R.A. Sheldon, Cu(II)-nitroxyl radicals as catalytic galactose oxidase mimics, Org. Biomol. Chem. 1 (2003) 3232–3237, https://doi.org/10.1039/b305941c.
[5] H. Alamgholiloo, S. Rostamnia, K. Zhang, T.H. Lee, Y.S. Lee, R.S. Varma, H. W. Jang, M. Shokouhimehr, Boosting aerobic oxidation of alcohols via synergistic effect between TEMPO and a composite Fe_3O_4/Cu-BDC/GO Nanocatalyst, ACS Omega 5 (2020) 5182–5191, https://doi.org/10.1021/acsomega.9b04209.
[6] E. Doustkhah, S. Rostamnia, B. Gholipour, B. Zeynizadeh, A. Baghban, R. Luque, Design of chitosan-dithiocarbamate magnetically separable catalytic nanocomposites for greener aqueous oxidations at room temperature, Mol. Catal. 434 (2017) 7–15, https://doi.org/10.1016/j.mcat.2017.01.031.
[7] P.J. Figiel, A. Sibaouih, J.U. Ahmad, M. Nieger, M.T. Räisänen, M. Leskelä, T. Repo, Aerobic oxidation of benzylic alcohols in water by 2,2,6,6- tetramethylpiperidine-1-oxyl(TEMPO)/Copper(II) 2-N-Arylpyrrolecarbaldimino complexes, Adv. Synth. Catal. 351 (2009) 2625–2632, https://doi.org/10.1002/adsc.200900478.
[8] Z. Hu, Y. Zhao, J. Liu, J. Wang, B. Zhang, X. Xiang, Ultrafine MnO_2 nanoparticles decorated on graphene oxide as a highly efficient and recyclable catalyst for aerobic oxidation of benzyl alcohol, J. Colloid Interface Sci. 483 (2016) 26–33, https://doi.org/10.1016/j.jcis.2016.08.010.
[9] S. Chen, G. Liu, H. Yadegari, H. Wang, S.Z. Qiao, Three-dimensional MnO_2 ultrathin nanosheet aerogels for high-performance LiO_2 batteries, J. Mater. Chem. A. 3 (2015) 2559–2563, https://doi.org/10.1039/c5ta00004a.
[10] Y. Murashima, R. Ohtani, T. Matsui, H. Takehira, R. Yokota, M. Nakamura, L. F. Lindoy, S. Hayami, Coexistence of electrical conductivity and ferromagnetism in a hybrid material formed from reduced graphene oxide and manganese oxide, Dalt. Trans. 44 (2015) 5049–5052, https://doi.org/10.1039/c5dt00299k.
[11] J. Qu, L. Shi, C. He, F. Gao, B. Li, Q. Zhou, H. Hu, G. Shao, X. Wang, J. Qiu, Highly efficient synthesis of graphene/MnO_2 hybrids and their application for ultrafast

oxidative decomposition of methylene blue, Carbon N. Y. 66 (2014) 485–492, https://doi.org/10.1016/j.carbon.2013.09.025.
[12] J. Lei, X. Lu, W. Wang, X. Bian, Y. Xue, C. Wang, L. Li, Fabrication of MnO_2/graphene oxide composite nanosheets and their application in hydrazine detection, RSC Adv 2 (2012) 2541–2544, https://doi.org/10.1039/c2ra01065h.
[13] Y. Dong, K. Li, P. Jiang, G. Wang, H. Miao, J. Zhang, C. Zhang, Simple hydrothermal preparation of α-, β-, and γ-MnO_2 and phase sensitivity in catalytic ozonation, RSC Adv 4 (2014) 39167–39173, https://doi.org/10.1039/c4ra02654c.
[14] Z. Li, Y. Ding, Y. Xiong, Q. Yang, Y. Xie, One-step solution-based catalytic route to fabricate novel α-MnO_2 hierarchical structures on a large scale, Chem. Commun. (2005) 918–920, https://doi.org/10.1039/b414204g.
[15] Z. Li, Y. Ding, Y. Xiong, Y. Xie, Rational growth of various α-MnO_2 hierarchical structures and β-MnO2 nanorods via a homogeneous catalytic route, Cryst. Growth Des. 5 (2005) 1953–1958, https://doi.org/10.1021/cg050221m.
[16] J. Wu, H. Huang, L. Yu, J. Hu, Controllable hydrothermal synthesis of MnO₂ nanostructures, Adv. Mater. Phys. Chem (2013) 201–205, https://doi.org/10.4236/ampc.2013.33029, 03.
[17] F. Cheng, J. Zhao, W. Song, C. Li, H. Ma, J. Chen, P. Shen, Facile controlled synthesis of MnO_2 nanostructures of novel shapes and their application in batteries, Inorg. Chem. 45 (2006) 2038–2044, https://doi.org/10.1021/ic051715b.
[18] M.M. Kadam, K.B. Dhopte, N. Jha, V.G. Gaikar, P.R. Nemade, Synthesis, characterization and application of γ-MnO_2/graphene oxide for the selective aerobic oxidation of benzyl alcohols to corresponding carbonyl compounds, New J. Chem. 40 (2016) 1436–1442, https://doi.org/10.1039/c5nj03140k.
[19] R.B. Tosun, K.Ö. Hamaloğlu, P.A. Kavaklı, C. Kavaklı, A. Tuncel, A synergistic catalyst based on a multivalence monodisperse-porous microspheres with oxygen vacancies for benzyl alcohol oxidation, Mol. Catal. 497 (2020), 111227, https://doi.org/10.1016/j.mcat.2020.111227.
[20] A. Kamimura, Y. Nozaki, M. Nishiyama, M. Nakayama, Oxidation of benzyl alcohols by semi-stoichiometric amounts of cobalt-doped birnessite-type layered MnO2 under oxygen atmosphere, RSC Adv. 3 (2013) 468–472, https://doi.org/10.1039/c2ra22117a.
[21] J. Bu, W. Wang, H. Zhang, C. Wu, B. Zhang, Y. Cao, F. Zhou, Q. Zhang, X. Zhang, Efficient synthesis of imine from alcohols and amines over different crystal structure MnOX catalysts, Mol. Catal. 459 (2018) 46–54, https://doi.org/10.1016/j.mcat.2018.08.016.
[22] Q. Tang, X. Huang, Y. Chen, T. Liu, Y. Yang, Characterization and catalytic application of highly dispersed manganese oxides supported on activated carbon, J. Mol. Catal. A Chem. 301 (2009) 24–30, https://doi.org/10.1016/j.molcata.2008.11.003.
[23] Y. Li, A. Sabbaghi, J. Huang, K.C. Li, L.S. Tsui, F.L.Y. Lam, X. Hu, Aerobic oxidation of benzyl alcohol: influence from catalysts basicity, acidity, and preparation methods, Mol. Catal. 485 (2020), 110789, https://doi.org/10.1016/j.mcat.2020.110789.
[24] A. Wang, W.Y. Zhou, Z. Sun, Z. Zhang, Z. Zhang, M.Y. He, Q. Chen, Mn(III) active site in hydrotalcite efficiently catalyzes the oxidation of alkylarenes with molecular oxygen, Mol. Catal. 499 (2021), 111276, https://doi.org/10.1016/j.mcat.2020.111276.
[25] D. Wu, X. Xie, Y. Zhang, D. Zhang, W. Du, X. Zhang, B. Wang, MnO_2/carbon composites for supercapacitor: synthesis and electrochemical performance, Front. Mater. 7 (2020) 1–16, https://doi.org/10.3389/fmats.2020.00002.
[26] H. Alamgholiloo, S. Rostamnia, N.N. Pesyan, Anchoring and stabilization of colloidal PdNPs on exfoliated bis-thiourea modified graphene oxide layers with super catalytic activity in water and PEG, Colloids Surfaces A Physicochem. Eng. Asp. 602 (2020), 125130, https://doi.org/10.1016/j.colsurfa.2020.125130.
[27] V.M. Shinde, E. Skupien, M. Makkee, Synthesis of highly dispersed Pd nanoparticles supported on multi-walled carbon nanotubes and their excellent catalytic performance for oxidation of benzyl alcohol, Catal. Sci. Technol. 5 (2015) 4144–4153, https://doi.org/10.1039/c5cy00563a.
[28] H. Alamgholiloo, S. Rostamnia, A. Hassankhani, X. Liu, A. Eftekhari, A. Hasanzadeh, K. Zhang, H. Karimi-Maleh, S. Khaksar, R.S. Varma, M. Shokouhimehr, Formation and stabilization of colloidal ultra-small palladium nanoparticles on diamine-modified Cr-MIL-101: synergic boost to hydrogen production from formic acid, J. Colloid Interface Sci. 567 (2020) 126–135, https://doi.org/10.1016/j.jcis.2020.01.087.
[29] G. Wu, Y. Gao, F. Ma, B. Zheng, L. Liu, H. Sun, W. Wu, Catalytic oxidation of benzyl alcohol over manganese oxide supported on MCM-41 zeolite, Chem. Eng. J. 271 (2015) 14–22, https://doi.org/10.1016/j.cej.2015.01.119.
[30] S. Dai, N. Wang, C. Qi, X. Wang, Y. Ma, L. Yang, X. Liu, Q. Huang, C. Nie, B. Hu, X. Wang, Preparation of core-shell structure Fe3O4@C@MnO2 nanoparticles for efficient elimination of U(VI) and Eu(III) ions, Sci. Total Environ. 685 (2019) 986–996, https://doi.org/10.1016/j.scitotenv.2019.06.292.
[31] Z. Fathi, E. Doustkhah, S. Rostamnia, F. Darvishi, A. Ghodsi, Y. Ide, Interaction of Yarrowia lipolytica lipase with dithiocarbamate modified magnetic carbon Fe3O4@C-NHCS2H core-shell nanoparticles, Int. J. Biol. Macromol. 117 (2018) 218–224, https://doi.org/10.1016/j.ijbiomac.2018.05.156.
[32] A. Ahadi, H. Alamgholiloo, S. Rostamnia, X. Liu, M. Shokouhimehr, D.A. Alonso, R. Luque, Layer-wise titania growth within dimeric organic functional group viologen periodic mesoporous organosilica as efficient photocatalyst for oxidative formic acid decomposition, ChemCatChem 11 (2019) 4803–4809, https://doi.org/10.1002/cctc.201900486.
[33] A. Baghban, M. Heidarizadeh, E. Doustkhah, S. Rostamnia, P.F. Rezaei, Covalently bonded pancreatic lipase onto the dithiocarbamate/chitosan-based magnetite: stepwise fabrication of Fe_3O_4@CS/NHCS-Lip as a novel and promising nanobiocatalyst, Int. J. Biol. Macromol. 103 (2017) 1194–1200, https://doi.org/10.1016/j.ijbiomac.2017.05.159.
[34] H. Karimi-Maleh, F. Karimi, S. Malekmohammadi, N. Zakariae, R. Esmaeili, S. Rostamnia, M.L. Yola, N. Atar, S. Movaghgharnezhad, S. Rajendran, A. Razmjou, Y. Orooji, S. Agarwal, V.K. Gupta, An amplified voltammetric sensor based on platinum nanoparticle/polyoxometalate/two-dimensional hexagonal boron nitride nanosheets composite and ionic liquid for determination of N-hydroxysuccinimide in water samples, J. Mol. Liq. (2020) 310, https://doi.org/10.1016/j.molliq.2020.113185.
[35] E. Doustkhah, M. Heidarizadeh, S. Rostamnia, A. Hassankhani, B. Kazemi, X. Liu, Copper immobilization on carboxylic acid-rich Fe_3O_4-Pectin: Cu2+@Fe_3O_4-Pectin a superparamagnetic nanobiopolymer source for click reaction, Mater. Lett. 216 (2018) 139–143, https://doi.org/10.1016/j.matlet.2018.01.014.
[36] Z. Li, Y. Yao, Y. Zheng, T. Gao, Z. Liu, G. Zhou, Fabrication of core-shell Fe_3O_4 @C@MnO_2 microspheres and their application in supercapacitors, J. Electrochem. Soc. 165 (2018), https://doi.org/10.1149/2.0961802jes. E58-E63.
[37] B. Duan, D. Wang, H. Wu, P. Xu, P. Jiang, G. Xia, Z. Liu, H. Wang, Z. Guo, Q. Chen, Core-Shell Structurized Fe_3O_4@C@MnO_2 nanoparticles as pH responsive T1-T2* dual-modal contrast agents for tumor diagnosis, ACS Biomater. Sci. Eng 4 (2018) 3047–3054, https://doi.org/10.1021/acsbiomaterials.8b00287.
[38] I.J. Bruce, T. Sen, Surface modification of magnetic nanoparticles with alkoxysilanes and their application in magnetic bioseparations, Langmuir 21 (2005) 7029–7035, https://doi.org/10.1021/la050553t.
[39] Y. Li, X. Xu, D. Qi, C. Deng, P. Yang, X. Zhang, Yan Li, † Xiuqing Xu, † Dawei Qi, Chunhui Deng, *Pengyuan Yang, Xiangmin Zhang*, J. Proteome Res. 7 (2008) 2526–2538.
[40] Y. Li, T. Leng, H. Lin, C. Deng, X. Xu, N. Yao, P. Yang, X. Zhang, Preparation of Fe_3O_4@ZrO_2 core - shell microspheres as affinity probes for selective enrichment and direct determination of phosphopeptides using matrix-assisted laser desorption ionization mass spectrometry, J. Proteome Res. 6 (2007) 4498–4510, https://doi.org/10.1021/pr070167s.
[41] X. Bao, Z. Qiang, J.H. Chang, W. Ben, J. Qu, Synthesis of carbon-coated magnetic nanocomposite (Fe_3O_4 at C) and its application for sulfonamide antibiotics removal from water, J. Environ. Sci. (China). 26 (2014) 962–969, https://doi.org/10.1016/S1001-0742(13)60485-4.
[42] F. Arena, B. Gumina, A.F. Lombardo, C. Espro, A. Patti, L. Spadaro, L. Spiccia, Nanostructured MnOx catalysts in the liquid phase selective oxidation of benzyl alcohol with oxygen: part I. Effects of Ce and Fe addition on structure and reactivity, Appl. Catal. B Environ. 162 (2015) 260–267, https://doi.org/10.1016/j.apcatb.2014.06.054.
[43] M. Alhumaimess, Z. Lin, Q. He, L. Lu, N. Dimitratos, N.F. Dummer, M. Conte, S. H. Taylor, J.K. Bartley, C.J. Kiely, G.J. Hutchings, Oxidation of benzyl alcohol and carbon monoxide using gold nanoparticles supported on MnO_2 nanowire microspheres,, Chem. A Eur. J. 20 (2014) 1701–1710, https://doi.org/10.1002/chem.201303355.
[44] V.G. Reddy, D. Jampaiah, A. Chalkidis, Y.M. Sabri, E.L.H. Mayes, S.K. Bhargava, Highly dispersed cobalt oxide nanoparticles on manganese oxide nanotubes for aerobic oxidation of benzyl alcohol, Catal. Commun. 130 (2019), 105763, https://doi.org/10.1016/j.catcom.2019.105763.
[45] I.M. Goldman, Observation of a large isotope effect in the manganese dioxide oxidation of benzyl alcohol, J. Org. Chem. 34 (1969) 3289–3295, https://doi.org/10.1021/jo01263a015.